ACS EARTH AND SPACE CHEMISTRY

http://pubs.acs.org/journal/aesccq

Article

Gas-Phase Formation and Isomerization Reactions of Cyanoacetaldehyde, a Prebiotic Molecule of Astrochemical Interest

Bernardo Ballotta,[‖] Surajit Nandi,[‖] Vincenzo Barone, and Sergio Rampino*

Cite This: *ACS Earth Space Chem.* 2021, 5, 1071−1082

Read Online

ACCESS | Metrics & More | Article Recommendations | Supporting Information

ABSTRACT: Cyanoacetaldehyde ($NC-CH_2CH=O$) is considered, together with guanidine and urea, as a precursor of the pyrimidine bases cytosine and uracil. Although it has not yet been detected in the interstellar medium (ISM), several hypotheses have been put forward about its synthesis in solution and in the gas phase. In this paper, we present a gas-phase model of the barrierless reaction between formyl (HCO) and cyanomethyl (CH_2CN) radicals leading to cyanoacetaldehyde and focus on its evolution through isomerization and dissociation pathways. The potential-energy surface for all reactions has been explored by DFT calculations employing double-hybrid functionals and further refined through the "Cheap" composite scheme. Our results indicate that the direct association of the two reacting radicals (HCO and CH_2CN) is strongly exothermic and thus thermodynamically favored under the harsh conditions of the ISM. Microcanonical rate constants computed with the help of the StarRate program for energies up to 6 kJ mol^{-1} above the dissociation limit show that the most abundant products are the two conformers of cyanoacetaldehyde (nitrile and carbonyl groups in a cis or trans configuration) which, despite having comparable stability, are obtained with a cis/trans ratio of 0.35:0.65. The formation of other products with relative abundances not exceeding 10% is also discussed.

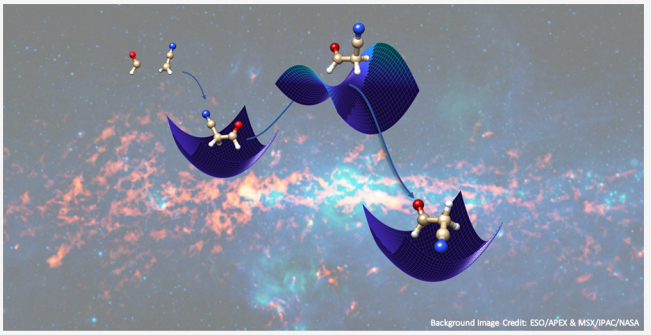

KEYWORDS: *astrochemistry, interstellar medium, complex organic molecules, cyanoacetaldehyde, potential energy surface, kinetics*

1. INTRODUCTION

The discovery of pyrimidine traces in carbonaceous meteorites in 1979 attracted a lot of attention to the study of possible synthetic pathways for this important scaffold of RNA and DNA bases. During the years, several models have been proposed and experiments have been performed in order to simulate conditions resembling those of the interstellar medium (ISM) or primitive Earth for the formation of molecules such as purine and pyrimidine from so-called complex organic molecules (COMs).

In this context, the involvement of cyanoacetaldehyde in the synthesis of the pyrimidine bases has been investigated for a long time. Early experimental studies in aqueous solution were performed already in 1968 by Ferris *et al.*,[1] who suggested a prebiotic synthesis of pyrimidine starting from cyanoacetylene and cyanate, because of their supposed high abundances in the primordial soup and, for HC_3N, also in Titan's atmosphere. However, a few years later (1973), Ferris *et al.*[2] described an alternative route to the formation of the same molecule starting from the condensation of cyanoacetaldehyde and guanidine to form 2,4-diaminopyrimidine that hydrolyzed to cytosine and uracil and suggested that this route might be favored with respect to the former one due to the lower tendency of cyanoacetaldehyde and guanidine (with respect to cyanoacetylene and cyanate) to react with other nucleophiles, thus featuring greater stability as starting materials.

Since then, several alternative synthetic routes to pyrimidine have been proposed, which included other cyanoacetaldehyde reaction partners such as urea.[3] Robertson and Miller[4] suggested to use concentrated urea solutions (similar to those found in evaporating lagoons or in pools on drying beaches on the early Earth) in order to favor the reaction with cyanoacetaldehyde to form cytosine in yields of 30−50%. Additionally, theoretical investigations have been undertaken to study the possible pyrimidine and purine synthetic routes.[5] For example, Kaur and Sharma[6] have performed computational simulations, using density-functional theory (DFT), of the possible free radical ammonia-mediated pathways for cytosine and uracil formation, where cyanoacetaldehyde plays a key role, and, more recently, a computational study of water-

Received: January 18, 2021
Revised: April 28, 2021
Accepted: April 29, 2021
Published: May 11, 2021

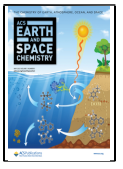

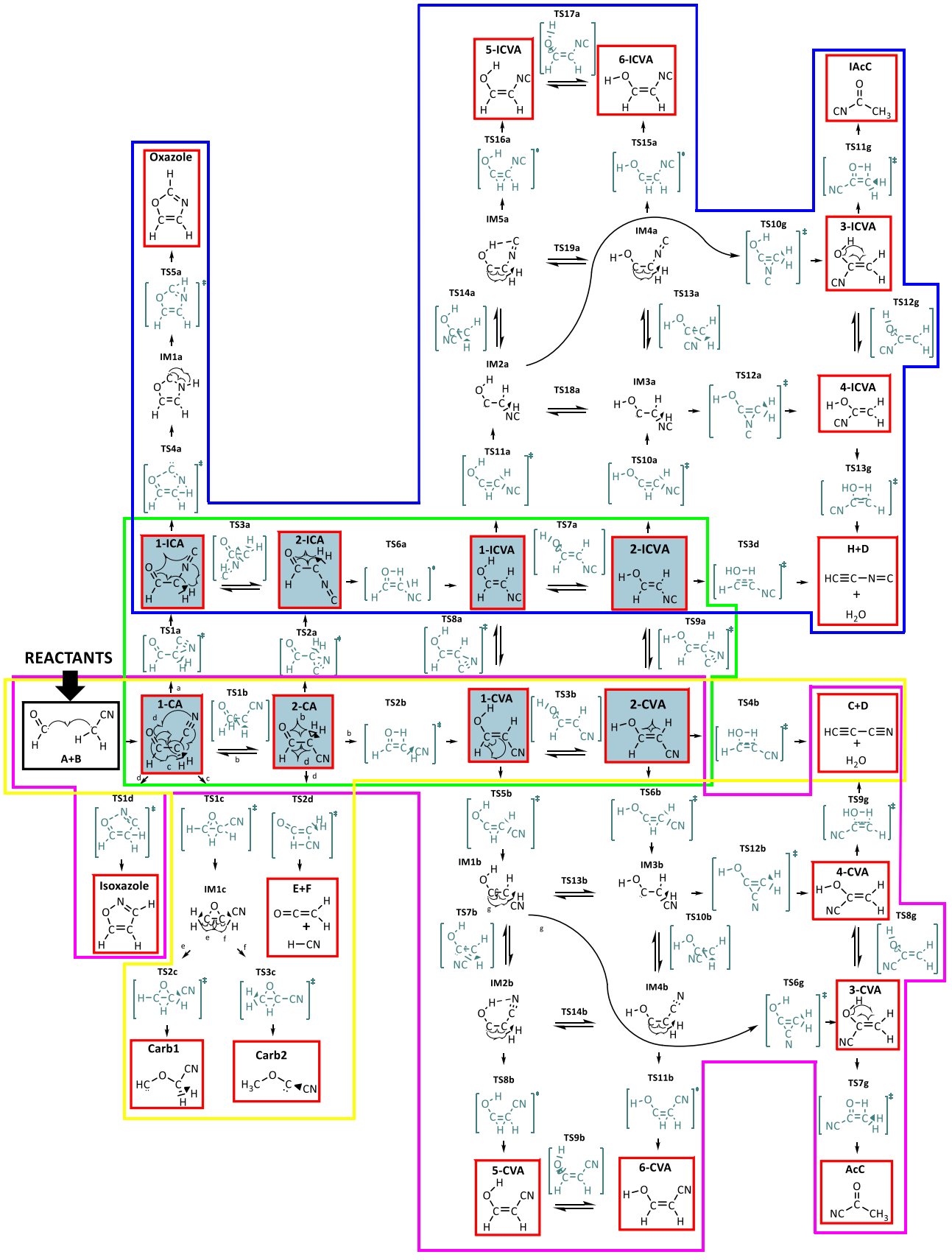

Figure 1. Comprehensive view of the reaction mechanism for the formation of cyanoacetaldehyde from the formyl and cyanomethyl radicals considered in this article.

https://doi.org/10.1021/acsearthspacechem.1c00013
ACS Earth Space Chem. 2021, 5, 1071−1082

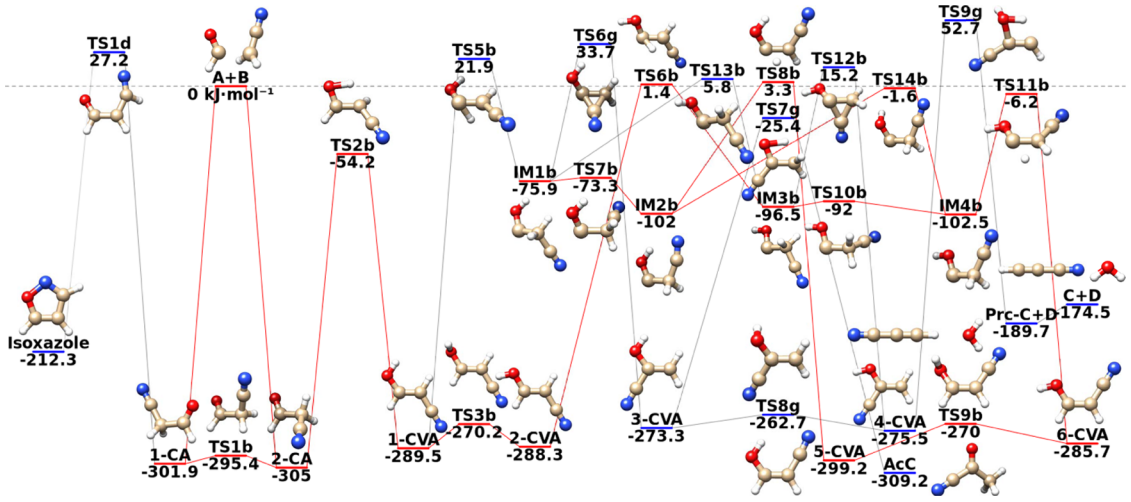

Figure 2. Energetics of the isomerization of cyanoacetaldehyde conformers (**1-CA**, **2-CA**), cyano vinyl alcohol isomers (**1-CVA**, **2-CVA**, **3-CVA**, **4-CVA**, **5-CVA**, **6-CVA**), **Isoxazole**, and **AcC**. Dissociation to cyanoacetylene and water (**C** + **D**) is also included. Energies in kJ mol^{-1} relative to the dissociation limit.

catalyzed synthetic route to pyrimidine bases starting from cyanoacetaldehyde and guanidine has been presented.[7]

Due to its relevance in the above discussed reactions, cyanoacetaldehyde (and its enolic isomers) has been the subject of computational and experimental IR[8] and microwave[9] spectroscopic characterization in order to facilitate its search in the ISM by comparison of laboratory spectra with those recorded by modern and powerful telescopes. These studies also showed that cyanoacetaldehyde conformers are more stable than the enolic isomers due to the presence of a nitrile group which weakly interacts with the hydrogen atom of the carbonyl group.

Despite all these efforts, cyanoacetaldehyde has not yet been detected in the ISM. A mandatory step for a better assessment of the role of this important molecule in the ISM is the investigation of the possible mechanisms for its formation. A computational study reported on a gas-phase model for the cyanoacetylene hydrolysis reaction, considered as a fundamental step for the formation of cyanoacetaldehyde.[10] However, the activation energy for the addition of water to the cyanoacetylene triple bond turned out to be too high, so that this reaction channel should be closed under the extreme conditions of primitive Earth and ISM. This led the authors to hypothesize a catalytic process on a grain surface, which is able to decrease the activation energy.

In the present study, we suggest an alternative mechanism for the formation of cyanoacetaldehyde, involving two radicals already detected in the ISM, namely, cyanomethyl (CH_2CN) and formyl (HCO), and focus on the chemical evolution of cyanoacetaldehyde. In particular, the isomerization mechanism of cyanoacetaldehyde and its cyano vinyl alcohol isomers, which are formed in equilibrium with cyanoacetaldehyde, is also analyzed. Moreover, some cyanoacetaldehyde dissociation reaction paths are investigated in order to determine if such dissociation products are more stable than cyanoacetaldehyde. Finally, in order to provide a quantitative picture of the reaction progress, we modeled the chemical kinetics of the reaction and computed the branching ratios for all the isomers and reaction products with the help of the StarRate computer program,[11,12] specifically designed to study astrochemical reactions.

The article is organized as follows. In Section 2, the computational methods are described. In Section 3, the computed reaction mechanism is discussed with reference to the stationary points of the potential-energy surface (PES). In Section 4, the kinetics of the reaction is addressed. Section 5 is devoted to conclusions and perspectives.

2. COMPUTATIONAL DETAILS

On the grounds of previous experience,[13−15] geometry optimizations and zero-point corrected electronic energies of reactants, transition states, intermediates, and products along the reaction pathways were obtained by the B2PLYP[16,17] -D3[18] double-hybrid functional in conjunction with the jun-cc-pVTZ basis set.[19] The stationary points on the reaction pathways were characterized as minima (reactants, intermediates, and products) and saddle points (transition states) based on vibrational frequency calculations. The transition states obtained were further confirmed using intrinsic reaction coordinate (IRC)[20] scans at the same levels of theory. For reference purposes, calculations were performed also using the rev-DSD-PBEP86[21] functional.

After that, for all stationary points computed with the B2PLYP-D3 functional, improved electronic energies were obtained by means of the "Cheap" composite method, which includes core−valence correlation energy and complete basis set extrapolation at the MP2[22] level on top of CCSD(T)[23] energies computed with a triple-zeta basis set[24−27] and has proven to provide absolute deviations from sophisticated HEAT-like composite schemes within 2 kJ mol^{-1}.[13,28] In detail

$$E_{\text{cheap}} = E^{\text{CCSD(T)/VTZ}} + \Delta E^{\text{MP2/CBS}} + \Delta E^{\text{MP2/CV}} \quad (1)$$

where

$$\Delta E^{\text{MP2/CBS}} = \frac{4^3 E^{\text{MP2/QZ}} - 3^3 E^{\text{MP2/TZ}}}{4^3 - 3^3} - E^{\text{MP2/TZ}} \quad (2)$$

and

$$\Delta E^{\text{MP2/CV}} = E^{\text{MP2/pCVTZ,a.e.}} - E^{\text{MP2/pCVTZ,f.c.}} \quad (3)$$

with $\Delta E^{\text{MP2/CV}}$ being the energy correction due to the core correlation evaluated at the MP2/cc-pCVTZ level. In eq 2, $\Delta E^{\text{MP2/CBS}}$ is the MP2 correlation energy extrapolated to the

https://doi.org/10.1021/acsearthspacechem.1c00013
ACS Earth Space Chem. 2021, 5, 1071−1082

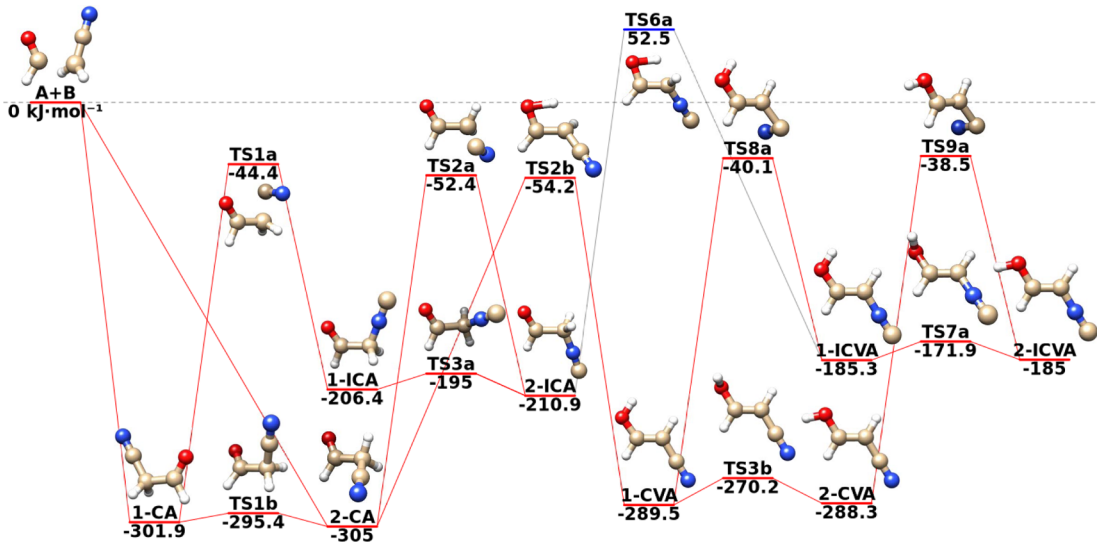

Figure 3. Energetics of the isomerization of cyanoacetaldehyde conformers (**1-CA**, **2-CA**) and cyano vinyl alcohol isomers (**1-CVA** and **2-CVA**) to isocyanoacetaldehyde conformers (**1-ICA** and **2-ICA**) and isocyano vinyl alcohol isomers (**1-ICVA** and **2-ICVA**). Energies in kJ mol^{-1} relative to the dissociation limit.

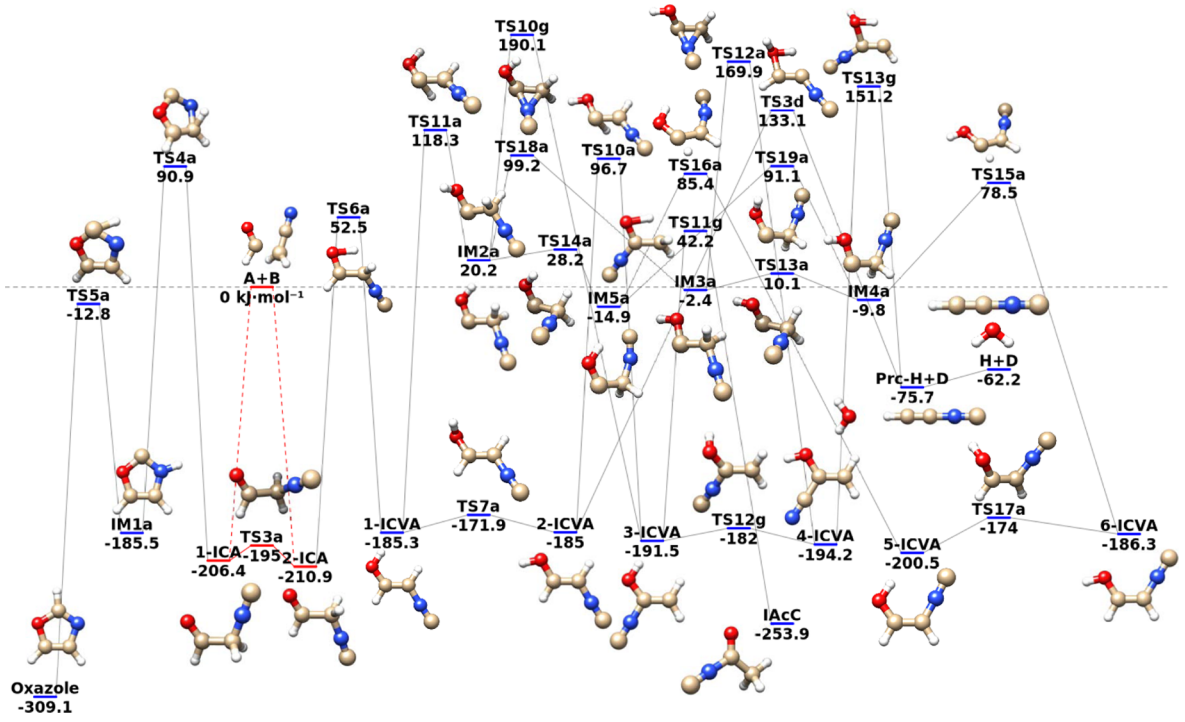

Figure 4. Energetics of the isomerization of isocyanoacetaldehyde conformers, isocyano vinyl alcohol isomers (**1-ICVA**, **2-ICVA**, **3-ICVA**, **4-ICVA**, **5-ICVA**, and **6-ICVA**), **Oxazole**, and **IAcC**. Dissociation to **H** + **D** also included. Energies in kJ mol^{-1} relative to the dissociation limit.

CBS limit by using n^{-3} extrapolation formula applied to the cc-pVTZ and cc-pVQZ basis sets.[29,30] A zero-point vibrational energy correction based on B2PLYP-D3 calculations was applied to "Cheap" electronic energies, and DFT vibrational frequencies obtained with the same functional were used for kinetics calculations. All B2PLYP and rev-DSD-PBEP86 calculations were performed using Gaussian09,[31] while "Cheap" calculations were performed using CFour.[32,33]

Kinetics calculations were performed as described in Section 4 with the help of the StarRate program[11,12] interfaced to the Gaussian code through a versatile XML interface (see also refs 34 and 35 on the issue of interoperability between electronic-structure and dynamics/kinetics programs).

3. POTENTIAL ENERGY SURFACE

We start the presentation of our results by illustrating the computed mechanism for the formation of cyanoacetaldehyde starting from two radicals widely detected in the ISM, namely, formyl (HCO) and cyanomethyl (CH_2CN). A large part of the possible isomerization and dissociation mechanisms of cyanoacetaldehyde has been included in the mechanism, which is shown in full in Figure 1. To simplify the analysis, the mechanism has been divided into four parts, whose

https://doi.org/10.1021/acsearthspacechem.1c00013
ACS Earth Space Chem. 2021, 5, 1071−1082

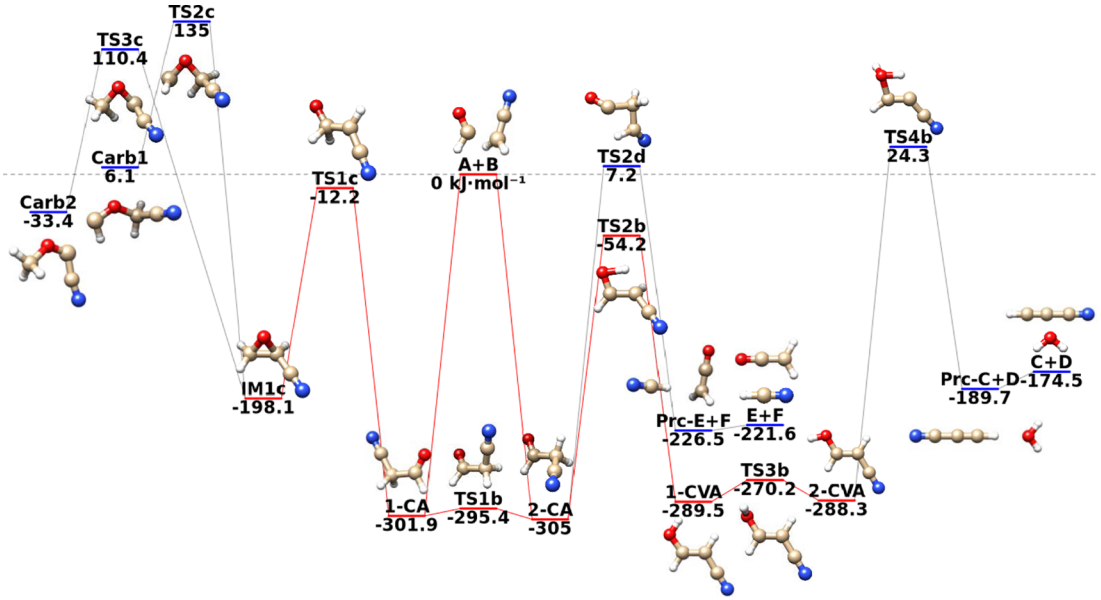

Figure 5. Energetics of the dissociation of cyanoacetaldehyde conformers (**1-CA** and **2-CA**) and cyano vinyl alcohol isomer (**2-CVA**). Energies in kJ mol^{-1} relative to the dissociation limit.

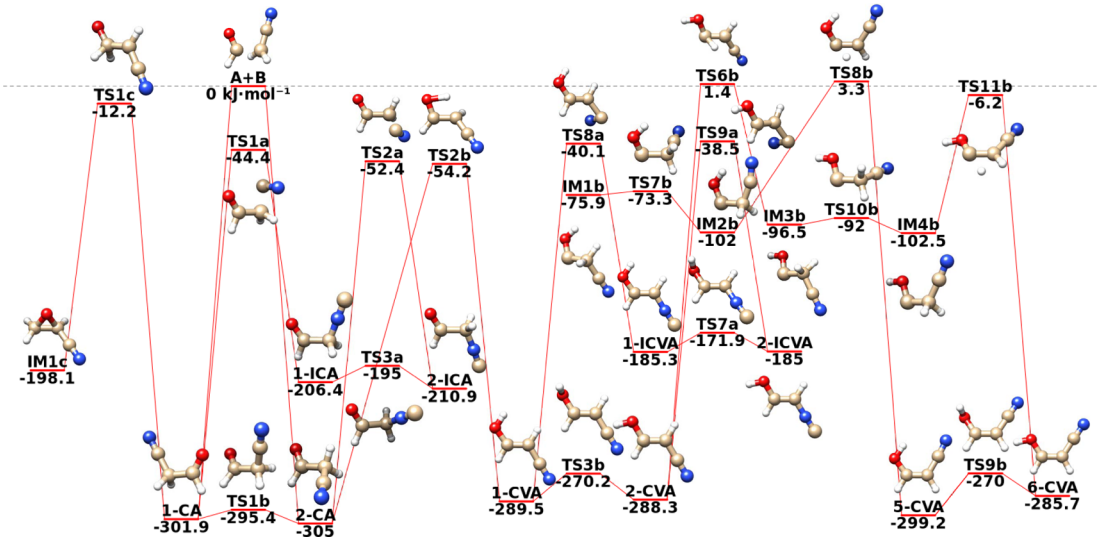

Figure 6. Comprehensive view of the astrochemically relevant paths (those highlighted in red in Figures 2−5) of the reaction scheme computed in this work.

reaction mechanisms and PES profiles are illustrated in Figures 2−5 and commented in the following. Then, the reaction paths in these four parts that are compatible with ISM conditions have been collected for a comprehensive view in Figure 6. Finally, the zero-point corrected energies of the species involved in the whole reaction are summarized in Table 1. Before moving to the analysis of the four parts of the overall reaction mechanism, we note that the rev-DSD-PBEP86 calculations outperform the B2PLYP ones when compared to "Cheap" data, as indicated by root-mean-square (rms) errors reported in the caption to Table 1.

3.1. Reaction Channel 1. Reaction channel 1 (violet frame in Figure 1) includes the association and isomerization reaction path of cyanoacetaldehyde conformers (**1-CA**, **2-CA**) to **Isoxazole**, acetylcyanide (**AcC**) and all the cyano vinyl alcohol isomers (**1-CVA**, **2-CVA**, **3-CVA**, **4-CVA**, **5-CVA**, **6-CVA**) obtained from keto-enolic tautomerization. The related mechanism and PES profile are reported in Figure 2. The **A** + **B** critical point in the reaction profile represents the reactant asymptote (algebraic sum of the zero-point corrected energies of the two radical fragments HCO and CH_2CN) or dissociation limit. In the following, all energies will be given relative to this value. The notation Prc in this and the following reaction schemes stands for a pre-reactive complex.

When the two reactants start to interact, they spontaneously give the two conformers **1-CA** at −301.9 kJ mol^{-1} and **2-CA** at −305.0 kJ mol^{-1}, depending on the initial relative orientation of the incoming radicals. The geometry optimization leads to a barrierless attack of the sp C eletrophillic center of HCO to the sp^2 C nucleophilic center in CH_2CN. **1-CA** is slightly less stable than **2-CA** probably due to a destabilizing repulsive electrostatic interaction between oxygen and nitrogen. Interconversion between the two conformers is possible

https://doi.org/10.1021/acsearthspacechem.1c00013
ACS Earth Space Chem. 2021, 5, 1071−1082

Table 1. Zero-point Corrected Energies (in kJ mol^{-1}) Relative to the Dissociation Limit for All the Species Involved in the HCO + CH_2CN Addition Reaction Computed Using the Three Different Levels of Theory Discussed in Section 2,[a]

	B2PLYP-D3	rev-DSD-PBEP86-D3	Cheap		B2PLYP-D3	rev-DSD-PBEP86-D3	Cheap
A + B	0	0	0	**TS2c**	151.4	132.1	135.0
1-CA	−290.3	−307.8	−301.9	**TS3c**	122.9	104.3	110.4
2-CA	−293.5	−310.7	−305.0	**TS1b**	−283.6	−300.9	−295.4
1-CVA	−279.5	−294.3	−289.5	**TS2b**	−48.9	−64.3	−54.2
2-CVA	−277.9	−292.6	−288.3	**TS3b**	−257.4	−272.4	−270.2
3-CVA	−259.8	−276.0	−273.3	**TS4b**	32.1	19.7	24.3
4-CVA	−262.0	−277.9	−275.5	**TS5b**	33.9	19.0	21.9
5-CVA	−289.0	−304.0	−299.2	**TS6b**	14.2	−1.4	1.4
6-CVA	−275.1	−289.9	−285.7	**TS7b**	−55.8	−72.0	−73.3
Prc-C + D	−180.7	−187.9	−189.7	**TS8b**	15.2	0.2	3.3
C + D	−164.0	−170.8	−174.5	**TS9b**	−248.2	−272.4	−270.0
Isoxazole	−198.0	−220.2	−212.3	**TS10b**	−73.6	−91.0	−92.0
AcC	−299.8	−316.5	−309.2	**TS11b**	6.0	−9.4	−6.2
Prc-E + F	−224.5	−230.8	−226.5	**TS12b**	24.8	8.4	15.2
E + F	−218.2	−223.8	−221.6	**TS13b**	24.2	9.2	5.8
Carb1	18.3	5.5	6.1	**TS14b**	15.6	0.6	−1.6
Carb2	−26.1	−37.1	−33.4	**TS6g**	42.4	26.6	33.7
IM1c	−183.8	−206.2	−198.1	**TS7g**	−22.2	−37.2	−25.4
IM1b	−58.6	−74.5	−75.9	**TS8g**	−248.2	−264.1	−262.7
IM2b	−84.7	−101.3	−102.0	**TS9g**	60.6	49.2	52.7
IM3b	−78.4	−95.5	−96.5	**TS10g**	200.7	190.0	190.1
IM4b	−84.7	−102.2	−102.5	**TS11g**	48.6	34.6	42.2
1-ICA	−193.5	−209.3	−206.4	**TS12g**	−165.4	−180.4	−182.0
2-ICA	−197.9	−213.6	−210.9	**TS13g**	144.2	150.5	151.2
1-ICVA	−172.5	−186.5	−185.3	**TS1a**	−30.9	−47.3	−44.4
2-ICVA	−171.7	−185.5	−185.0	**TS2a**	−39.9	−55.9	−52.4
3-ICVA	−176.0	−191.1	−191.5	**TS3a**	−181.2	−197.1	−195.0
4-ICVA	−178.5	−193.4	−194.2	**TS4a**	104.9	84.7	90.9
5-ICVA	−187.4	−201.6	−200.5	**TS5a**	4.3	−17.6	−12.8
6-ICVA	−173.1	−187.0	−186.3	**TS6a**	59.5	45.4	52.5
Prc-H + D	−64.0	−69.5	−75.7	**TS7a**	−156.7	−170.8	−171.9
H + D	−49.3	−54.5	−62.2	**TS8a**	−25.9	−39.2	−40.1
Oxazole	−291.9	−314.7	−309.1	**TS9a**	−24.1	−37.5	−38.5
IAcC	−242.5	−258.1	−253.9	**TS10a**	111.3	97.2	96.7
IM1a	−165.0	−187.1	−185.5	**TS11a**	132.1	118.6	118.3
IM2a	39.0	24.6	20.2	**TS12a**	181.6	170.4	169.9
IM3a	17.1	1.4	−2.4	**TS13a**	30.4	14.3	10.1
IM4a	8.6	−7.1	−9.8	**TS14a**	47.7	32.9	28.2
IM5a	3.0	−11.9	−14.9	**TS15a**	92.2	78.2	78.5
TS1d	40.3	42.8	27.2	**TS16a**	99.1	85.5	85.4
TS2d	10.7	−3.1	7.2	**TS17a**	−159.0	−173.1	−174.0
TS3d	144.3	132.9	133.1	**TS18a**	119.0	105.5	99.2
TS1c	17.7	13.1	−12.2	**TS19a**	108.6	95.4	91.1

[a]The RMS deviation of B2PLYP-D3 and rev-DSD-PBEP86-D3 data from Cheap values is 14.0 and 5.3 kJ mol^{-1}, respectively.

through rotation around the C−C single bond (through **TS1b** with an energy of −295.4 kJ mol^{-1}).

As already mentioned, also the isomerization process from **1-CA** to **Isoxazole** has been studied. The transition state **TS1d**, involving the simultaneous transposition of the hydrogen from methylene to the nitrile carbon and the attack of the nitrile carbon by carbonyl oxygen, has been found at 27.2 kJ mol^{-1} above the reactant asymptote, which makes this pathway unlikely in the ISM.

2-CA can give keto-enolic tautomerization to **1-CVA** through **TS2b** (involving transposition of the hydrogen from methylene to the carbonyl oxygen) that lies at −54.2 kJ mol^{-1}.

From **1-CVA**, two further isomerization pathways have been explored, related to the conformational isomerization toward **2-CVA** through **TS3b** and the isomerization process toward the carbenic intermediate **IM1b** through **TS5b**. According to our calculations, only the first isomerization process can occur in the ISM because **TS3b** lies below the asymptotic limit at −270.2 kJ mol^{-1}. The other isomerization process cannot occur because **TS5b** lies 21.9 kJ mol^{-1} above the dissociation limit.

Finally, several other isomerization processes have been studied, such as the formation of **3-CVA**, **4-CVA** (plus its dissociation to **C + D**), **5-CVA**, **6-CVA**, and **AcC**. Only the two conformers, **6-CVA** and **5-CVA**, can be formed through a complex isomerization pathway, which involves a relatively high energy transition state **TS6b** lying at 1.4 kJ mol^{-1} and two carbenic intermediates **IM3b** and **IM4b**. However, this is not

https://doi.org/10.1021/acsearthspacechem.1c00013
ACS Earth Space Chem. 2021, 5, 1071−1082

expected to be an efficient path as it involves a relatively high energy barrier of 289.7 kJ mol^{-1}.

3.2. Reaction Channel 2. Reaction channel 2 (green frame in Figure 1) involves the conversion, through isomerization reactions, of cyano compounds to related isocyano compounds. Mechanisms and the PES profile are given in Figure 3.

We found that most of the stationary points ruling this reaction channel lie below the dissociation limit, thus offering competitive reaction paths with respect to the isomerization mechanisms of the reaction channel 1. In analogy with channel 1, also in channel 2, the initial barrierless attack of the two reactants to give **1-CA** and **2-CA** and the keto-enolic tautomerization process to give **1-CVA** and **2-CVA** are included in order to make the explanation of the mechanism clearer.

Starting from **1-CA** and **2-CA**, two isomerization processes were computed to give **1-ICA** at −206.4 kJ mol^{-1} and **2-ICA** at −210.9 kJ mol^{-1}. **2-ICA** is slightly more stable than **1-ICA** probably due to a destabilizing repulsive electrostatic interaction between oxygen and nitrogen in the latter species. Two transition states, **TS1a** and **TS2a**, related to the nitrile/isonitrile isomerization processes, have been found at −44.4 kJ mol^{-1} and at −52.4 kJ mol^{-1}. Also in this case, the interconversion between **1-ICA** and **2-ICA** has been studied. The conformational transition state, **TS3a**, related to the interconversion process, has been found at −195.0 kJ mol^{-1}.

Moreover, the isomerization from isocyanoacetaldehyde (**2-ICA**) to isocyano vinyl alcohol (**1-ICVA**) has been investigated. Two possible pathways have been considered: the keto-enolic tautomerization reaction from **2-ICA** to **1-ICVA** through **TS6a** and the isomerization from **1-CVA** to **1-ICVA** through **TS8a**. Based on our calculations, only the second pathway can occur in ISM conditions because **TS8a** lies at −40.1 kJ mol^{-1} (**TS6a** shows instead an energy of 52.5 kJ mol^{-1}).

Finally, the conformational isomerization of **1-ICVA** into **2-ICVA** has been examined through two possible pathways: the rotation around the dihedral angle included by HOCC, from **1-ICVA** to **2-ICVA** through **TS7a**, and the nitrile/isonitrile isomerization from **2-CVA** to **2-ICVA** through **TS9a**. Both pathways can take place in the ISM as none of them exhibits an energy barrier above the reactant asymptote.

3.3. Reaction Channel 3. Reaction channel 3 (blue frame in Figure 1) includes the isomerization mechanisms of isocyanoacetaldehyde conformers (**1-ICA** and **2-ICA**) to **Oxazole**, acetyl isocyanide (**IAcC**) and all isocyano vinyl alcohol isomers (**1-ICVA**, **2-ICVA**, **3-ICVA**, **4-ICVA**, **5-ICVA**, and **6-ICVA**) obtained from the keto-enolic tautomerization. Furthermore, the dissociation path from **2-ICVA** to **H** + **D** and the isomerization of **3-ICVA** into **IAcC** are included. The reaction mechanism and the PES profile are given in Figure 4, where the dashed lines connecting **A** + **B** to **1-ICA** and **2-ICA** indicate that formation of isocyanoacetaldehyde from the reactants is indirect and proceeds through steps that are not shown in the scheme and that have been discussed in the previous subsections.

Based on our calculations, none of the above-mentioned pathways can take place in the ISM because too high energy barriers are involved.

3.4. Reaction Channel 4. Reaction channel 4 (yellow frame in Figure 1) includes some of the possible dissociation reactions of cyanoacetaldehyde to compounds already detected in the ISM such as ketene and hydrogen cyanide (**E** + **F**), cyanoacetylene and water (**C** + **D**), together with an isomerization reaction leading to the formation of carbene compounds (**Carb1**, **Carb2**). Reaction mechanisms and the PES profile are given in Figure 5.

This portion of the reaction mechanism thus features another isomerization reaction and two dissociation mechanisms. The isomerization reaction leads to the formation of two carbenic compounds **Carb1** and **Carb2** as possible products of a combustion process, however, very unlikely at the ISM conditions. On the other hand, **IM1c**, also known as oxiranecarbonitrile,[36] can be populated because **TS1c** lies 12.2 kJ mol^{-1} below the reactants.

The two dissociation mechanisms (to **C** + **D** and **E** + **F**) lead to the formation of other species widely detected in the ISM: ketene (H_2C_2O), hydrogen cyanide (HCN), cyanoacetylene (HC_3N), and water (H_2O). However, also for such paths, too high energy barriers were found.

Some additional remarks are in order about the dissociation mechanism which leads to HC_3N + H_2O since our results point out some differences with respect to the pathways proposed by Horn *et al.*[10] As already mentioned, those authors studied the formation of cyanoacetaldehyde from the cyanoacetylene (HC_3N) hydrolysis, concluding that **1-CVA** is the favored product issuing from the attack of H_2O to HC_3N. We carried out an IRC computation in order to verify which conformer is preferred upon addition of H_2O to HC_3N. According to our computations, **2-CVA** is the preferred conformer. Moreover, Horn *et al.* proposed a conversion from a cis to a trans configuration, which leads to a very unstable transition state. After that, from **1-CVA**, they found a transition state ruling the keto-enolic tautomerization, which leads to the formation of **2-CA**. Our calculations suggest that this is not the most efficient mechanism for the keto-enolic tautomerization reactions. As an alternative, we propose that the cis/trans isomerization is not needed to obtain **2-CA** but, rather, that **2-CVA** isomerizes to **1-CVA** and then to **2-CA**. This path does not involve the high-energy transition state ruling the cis/trans isomerization. In addition, the comparison of the reaction profile shows a good agreement of the energy barriers involved in both mechanisms, which confirms the validity of our computational procedure.

Two further dissociative pathways involving the breaking of C−C, C−O, and C−H bonds and leading to astrochemically relevant species were also investigated (though they are not shown in the figure). The first of these involves the dissociation of **6-CVA** to HOCN (cyanic acid) and HCCH (acetylene), two species that have already been detected in the ISM. The second one involves the dissociation of **1-CA** to NCHCCO (cyanoketene, not yet detected in the ISM) and H_2. Both pathways proceed through formation of a transition state and a pre-reactive complex. However, in both cases, the transition state lies significantly above the reactant asymptotic limit (120.2 and 18.5 kJ mol^{-1}, respectively), so that both processes have no relevance in the ISM conditions.

4. KINETICS

The potential energy surface for the reaction of cyanomethyl and formyl radicals computed in this work and presented in Section 3 gives an in-depth view of the overall mechanism of formation of cyanoacetaldehyde and its possible evolution. However, a comprehensive understanding of the evolution of the reaction along competitive paths can only be attained by

https://doi.org/10.1021/acsearthspacechem.1c00013
ACS Earth Space Chem. 2021, 5, 1071−1082

modeling the associated reaction kinetics, which provides a detailed description of the reaction progress and helps in predicting the chemical traces that might be detected experimentally in interstellar space.

In principle, the time evolution of a chemical reaction should be addressed through a quantum treatment of the underlying nuclear motion. However, exact quantum-dynamics calculations are only achievable for very small systems.[37−40] Approximate quantum-dynamical methods are able to extend this limit to slightly larger systems but are definitely out of reach for the reactions such as that reported in this article. More affordable, yet reasonably accurate, approaches are either a (quasi-)classical treatment[41−43] of the nuclear motion or simpler approximations rooted into some flavor of the transition-state theory (TST), where the kinetic information is obtained from the stationary points characterizing the PES. In the present case, the branching ratios among the several reaction products were obtained from unimolecular kinetics calculations in the Rice−Ramsperger−Kassel−Marcus framework[44−46] for all the steps following the bimolecular association. The reaction rates issuing from those computations are next combined in a master equation treatment. The microcanonical rate constants ($k(E)$) of each unimolecular step are given by

$$k(E) = \frac{N^{\ddagger}(E)}{h\rho(E)} \tag{4}$$

where E is the energy, $N^{\ddagger}(E)$ is the rovibrational sum of states of the transition state, h is Planck's constant, and $\rho(E)$ is the rovibrational density of states of the reactant species. The vibrational densities of states were calculated by the Stein−Rabinovitch algorithm[47] and are then convoluted with classical rotor densities of states to obtain the final rovibrational densities. Sums of states were computed by a simple integration of the corresponding densities. Then, the chemical master equation is constructed by using all the individual rate constants for each step. In this framework, the evolution of the relative abundance of each involved species as a function of time can be described by an ordinary first-order differential equation

$$\frac{\mathrm{d}\mathbf{c}(t)}{\mathrm{d}t} = \mathbf{K}\mathbf{c}(t) \tag{5}$$

where $\mathbf{c}(t)$ is the vector of the concentration of the species at time t and $\mathbf{K}$ is a square matrix containing proper combinations of the microcanonical rate constants for each step at a given energy. Accordingly, the time evolution of the species concentrations can be obtained by matrix diagonalization techniques and expressed as

$$\mathbf{c}(t) = \mathbf{Z}\, \mathrm{e}^{\mathbf{\Lambda} t}\, \mathbf{Z}^{-1}\mathbf{c}(0) \tag{6}$$

where $c(0)$ is the species concentration at $t = 0$, $\mathbf{\Lambda}$ is the eigenvalue vector, and $\mathbf{Z}$ is the eigenvector matrix. The readers are referred to refs 11 and 12 for further details about the implementation in StarRate.

As described in detail in Section 3, the title reaction starts with formation of **1-CA** from association of cyanomethyl (CH_2CN) and formyl radicals (HCO). This species can isomerize to **2-CA**, and both isomers can further evolve along several different pathways. Several reaction channels are, however, ruled by energy barriers lying above the reactant asymptote, thus being unlikely in the ISM. According to the results discussed in the preceding sections, only the following species can be formed by reactions involving only submerged barriers: **1-CA**, **2-CA**, **1-CVA**, **2-CVA**, **1-ICA**, **2-ICA**, **1-ICVA**, **2-ICVA**, and **IM1c**. This last species, however, is far less relevant than the others as it is accessed by a reaction step from **1-CA** through **TS1c** involving a very high energy barrier (289.7 kJ mol^{-1}).

In order to investigate the kinetics of the isomerization reactions of cyanoacetaldehyde, we addressed an energy range from 0 to 6 kJ mol^{-1} (equivalent temperature 720 K), corresponding to the typical accuracy of popular composite schemes and representing a conservative upper bound to the accuracy of the computed energy barriers. In the following, we first show for illustrative purposes the time evolution of the relative abundances of the several involved species for a selected energy of 5 kJ mol^{-1} (enough to open up a "non-submerged" reaction path) and then discuss the final populations (those resulting in the infinite future) over the entire considered energy range.

As shown in Figure 6, at 5 kJ mol^{-1}, additional reaction channels open up, leading to (1) formation of **5-CVA** and **6-CVA** through **TS6b** (lying at 1.4 kJ mol^{-1}), **IM3b**, and **IM4b**, and (2) formation of **IM1b** and **IM2b** through **TS8b** (lying at 3.3 kJ mol^{-1}). Among these species, only **5-CVA** and **6-CVA** turned out to be non-negligibly involved in the reaction, while all others (including the previously mentioned **IM1c**) resulted in relative abundances well below 0.1%. We will therefore from now on focus our analysis on the following 10 species: **1-CA**, **2-CA**, **1-CVA**, **2-CVA**, **1-ICA**, **2-ICA**, **1-ICVA**, **2-ICVA**, **5-CVA**, and **6-CVA**.

In Figure 7, the relative abundance of the ten main products outlined above is plotted as a function of time in a very short

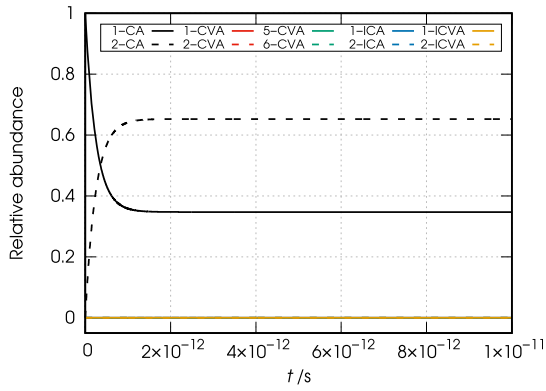

Figure 7. Relative abundance (arbitrary unit) *vs* time plot at 5 kJ mol^{-1}.

time frame at the beginning of the reaction (10^{-11} s) for an energy of 5 kJ mol^{-1}. The figure shows that rapidly (in a time frame of less than 2×10^{-12} s), the **1-CA**-**2-CA** isomerization process occurs (in agreement with its very low activation energy) and a **1-CA**:**2-CA** ratio of 0.35:0.65 is soon established.

This picture undergoes slight changes when moving to the analysis of a larger time frame. In the left panel of Figure 8, the relative abundances for the same species at the same energy of 5 kJ mol^{-1} are plotted as a function of time up to 6 s. The right panel reproduces the same plot using a logarithm scale for both axes. In this figure, the detail on the conversion between **1-CA** and **2-CA** is lost, but additional information is gained on the

https://doi.org/10.1021/acsearthspacechem.1c00013
ACS Earth Space Chem. 2021, 5, 1071−1082

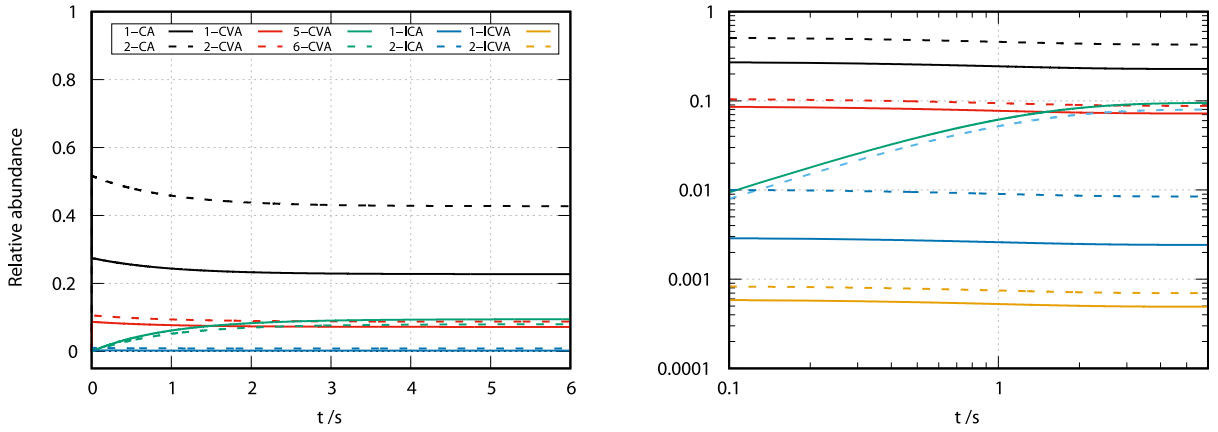

Figure 8. Relative abundance (arbitrary unit) *vs* time plot at 5 kJ mol^{-1}.

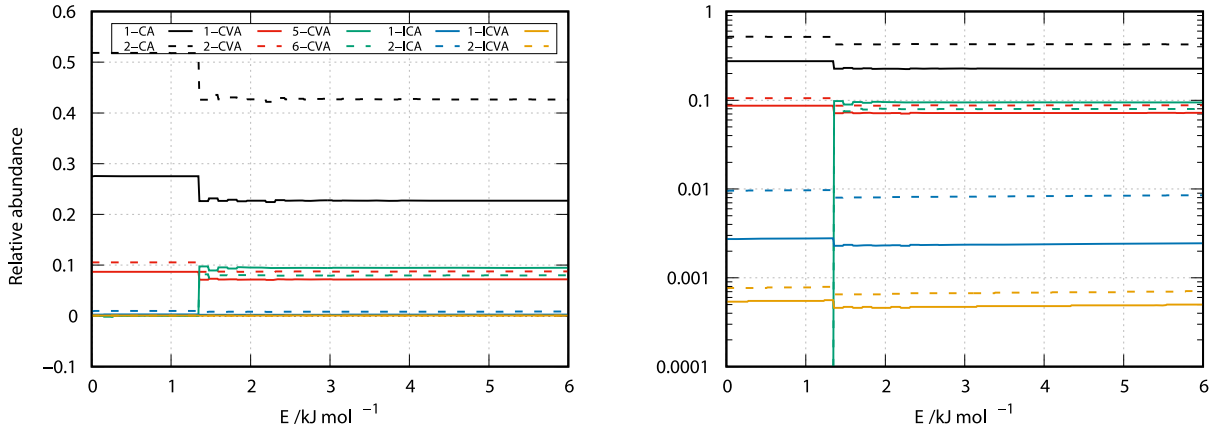

Figure 9. Final populations for all the species for an energy range of 6 kJ mol^{-1} above the dissociation limit.

progress of the overall reaction. In fact, as more visible in the right panel of the figure, formation of other species occurs at different time scales, whereby, for instance, **1-ICA** and **2-ICA** rapidly reach a relative abundance of ∼10%, while those of **5-CVA** and **6-CVA** reach a comparable plateau only after about 2 s. The relative abundance of **1-CA** and **2-CA** is of course affected by the population of the other species as the reaction proceeds (decreasing to values of 0.23 and 0.43, respectively); however, their ratio remains almost constant at a value of 0.35:0.65.

In order to assess how these results are affected by the available energy and obtain a more informative picture, we plot in the left section of Figure 9 the final populations for an energy range up to 6 kJ mol^{-1} (corresponding, as already mentioned, to an upper bound for the accuracy of the computed energy barriers). The right panel of the figure shows the same plot using a logarithm scale for the relative abundances. It is apparent that the picture is essentially the same for all considered energies, with the relative abundance of **2-CA** almost doubling that of **1-CA,** and the relative abundances of the minor species undergoing minor changes, except near an energy of 1.4 kJ mol^{-1} where the channel leading to formation of **5-CVA** and **6-CVA** opens up.

According to these results, the ratio between the abundances of the two main conformers **1-CA** and **2-CA** is far from thermodynamic equilibrium under the physical conditions characterizing the ISM. In fact, while the thermodynamic **1-CA:2-CA** ratio (which can be straightforwardly determined by the energy difference between the conformers) is 0.42:0.58 at a temperature of 10 K and 0.47:0.53 at a temperature of 24 K, the kinetically determined one keeps an almost constant value of about 0.35:0.65 in an energy range up to an equivalent temperature of 720 K.

Of course, the lack of collisional relaxation processes in the ISM due to low-pressure conditions implies that the effective formation of the discussed complexes entirely relies on radiative stabilization mechanisms.[48,49] These have indeed been shown to play a key role in association reactions, leading to complexes with several number of vibrational modes and accessible isomers[50] such as those targeted in this work. Vuitton *et al.*[51] have estimated that at low temperatures, the rate coefficients for exothermic processes leading to radiative association are close to the collision limit for adducts having as few as four C atoms, predicting an association rate of 1.1 × 10^{-10} cm^3 s^{-1} at 150 K for complexes having five "heavy" atoms such as cyanoacetaldehyde.

As pointed out in ref 49, in the low-pressure limit, the effective association rate is given by $k_{eff} = k_f k_r/(k_b + k_r)$, where k_f is the forward association rate, k_b is the back-dissociation rate, and k_r is the radiative stabilization rate. In order to assess the importance of radiative stabilization for the reaction considered in this work, we computed the **1-CA** association rate (forward rate, k_f) using a capture model for a long range potential of the form $-C_6/R^6$ using the approach outlined in ref 52. To this purpose, a C_6 coefficient of 182.92 E_H a_0^6 was obtained by performing energy calculations for several points along the entrance coordinate for the HCO + CH_2CN reaction and by fitting the energies to a $V = V_0 - C_6/R^6$ law. An

https://doi.org/10.1021/acsearthspacechem.1c00013
ACS Earth Space Chem. 2021, 5, 1071−1082

estimate of the rate constant for radiative stabilization (k_r) was obtained within a harmonic approximation from the ir absorption intensities for the $v = 0$ to $v = 1$ transition of the various vibrational modes of the complex as described in ref 49.

In an energy range of 0.12−1.32 kJ mol^{-1} (range of equivalent temperatures: 15−160 K), k_f varies from 3.5 × 10^{-10} to 4.8 × 10^{-10} cm^3 s^{-1}. On the other hand, the k_r calculated on the corresponding interval of equivalent temperatures ranges from 4.68 × 10^{-9} to 9.5 × 10^{-4} s^{-1}. Now, as can be argued from the above expression of k_{eff}, any value of k_b significantly lower than k_r (up to the limiting case of $k_b = 1.0 \times 10^{-23}$ and 5.1 × 10^{-21} s^{-1} obtained for the extremes of the mentioned energy range by computing k_b from k_f through the principle of detailed balance as done in ref 52) would lead to a rate equal to k_f. Thus, in the considered astrochemically relevant energy range, the effective association rate for the process studied in this work is expected to be in the range 3.5−4.8 × 10^{-10} cm^3 s^{-1}, which is in good agreement with the prediction by Vuitton et al. of 1.1 × 10^{-10} cm^3 s^{-1} at 150 K.[51]

5. CONCLUSIONS

In this paper, we have modeled a gas-phase route leading to the formation of cyanoacetaldehyde, an important molecule considered a forerunner of the pyrimidine bases cytosine and uracil. The computed mechanism starts from reaction of the formyl (HCO) and cyanomethyl (CH_2CN) radicals and involves several isomerization and dissociation pathways. The potential-energy surface for such reaction has been explored by quantum chemical computations employing double-hybrid density functionals and further refined by single-point calculations exploiting the "Cheap" composite scheme. According to our results, the direct association of the HCO and CH_2CN radicals is strongly exothermic and thus thermodynamically favoured under the harsh conditions of the ISM. Kinetic calculations show that the main products of the reaction are the two conformers of cyanoacetaldehyde (nitrile and carbonyl groups in a cis or a trans configuration) in a cis/trans ratio of about 0.35:0.65 (resulting from relative abundances of 0.28 and 0.52, respectively, in an energy range below 1.4 kJ mol^{-1}) for energy ranges compatible with the ISM conditions. Some other products are also found, including isomers of isocyanoacetaldehyde, cyano vinyl alcohol, and isocyano vinyl alcohol with relative abundances not exceeding 10%.

The computed ratio between the two main conformers of cyanoacetaldehyde differs from that computed at thermodynamical equilibrium and reflects the complexity of the overall reaction mechanism. Such ratio in the effective conditions of the ISM may be further affected by different destruction rates for the two conformers by reaction with the abundant atomic hydrogen, as shown for the much simpler case of *Z*- and *E*-cyanomethanimine in ref 53. This prompts further work, which is ongoing in our group for examining this aspect through the modeling of the more challenging reaction of cyanoacetaldehyde with atomic hydrogen.

■ ASSOCIATED CONTENT

Supporting Information

The Supporting Information is available free of charge at https://pubs.acs.org/doi/10.1021/acsearthspacechem.1c00013.

Cartesian coordinates in Å of each optimized structure (PDF)

Numerical data for Figure 7 (TXT)

Numerical data for Figure 8 (TXT)

Numerical data for Figure 9 (TXT)

■ AUTHOR INFORMATION

Corresponding Author

Sergio Rampino − *SMART Laboratory, Scuola Normale Superiore, Pisa 56126, Italy; Istituto Nazionale di Fisica Nucleare, Sezione di Pisa, Pisa 56127, Italy;* orcid.org/0000-0001-8525-7777; Email: sergio.rampino@sns.it

Authors

Bernardo Ballotta − *SMART Laboratory, Scuola Normale Superiore, Pisa 56126, Italy*

Surajit Nandi − *SMART Laboratory, Scuola Normale Superiore, Pisa 56126, Italy;* orcid.org/0000-0002-7105-2209

Vincenzo Barone − *SMART Laboratory, Scuola Normale Superiore, Pisa 56126, Italy; Istituto Nazionale di Fisica Nucleare, Sezione di Pisa, Pisa 56127, Italy;* orcid.org/0000-0001-6420-4107

Complete contact information is available at: https://pubs.acs.org/10.1021/acsearthspacechem.1c00013

Author Contributions

‖B.B. and S.N. contributed equally to this work.

Notes

The authors declare no competing financial interest.

■ ACKNOWLEDGMENTS

The research leading to these results has received funding from Scuola Normale Superiore through the project "DIVE: Development of Immersive approaches for the analysis of chemical bonding through Virtual-reality Environments" (SNS18_B_RAMPINO) and the program "Finanziamento a supporto della ricerca di base" (SNS_RB_RAMPINO), from the Italian Ministry of University and Research ("PRIN 2017", Grant Number 2017A4XRCA), and from the Italian Space Agency (ASI; "Life in Space" project, N. 2019-3-U.0).

■ REFERENCES

(1) Ferris, J. P.; Sanchez, R. A.; Orgel, L. E. Studies in prebiotic synthesis: III. Synthesis of pyrimidines from cyanoacetylene and cyanate. *J. Mol. Biol.* **1968**, *33*, 693−704.

(2) Ferris, J. P.; Zamek, O. S.; Altbuch, A. M.; Freiman, H. Chemical Evolution: XVIII. Synthesis of Pyrimidines from Guanidine and Cyanoacetaldehyde. *J. Mol. Evol.* **1974**, *3*, 301−309.

(3) Nelson, K. E.; Robertson, M. P.; Levy, M.; Miller, S. L. Concentration by Evaporation and the Prebiotic Synthesis of Cytosine. *Orig. Life Evol. Biosph.* **2001**, *31*, 221−229.

(4) Robertson, M. P.; Miller, S. L. An efficient prebiotic synthesis of cytosine and uracil. *Nature* **1995**, *375*, 772−774.

(5) Wang, T.; Bowie, J. H. Can cytosine, thymine and uracil be formed in interstellar regions? A theoretical study. *Org. Biomol. Chem.* **2012**, *10*, 652−662.

(6) Kaur, S.; Sharma, P. Cyanoacetaldehyde as a building block for prebiotic formation of pyrimidines. *Int. J. Quantum Chem.* **2019**, *119*, No. e25886.

(7) Choe, J. C. Formation of Cytosine and Uracil from Cyanoacetylaldehyde and Guanidine: A Computational Study. *Bull. Korean Chem. Soc.* **2020**, *41*, 382−384.

(8) Benidar, A.; Georges, R.; Guillemin, J. C.; Mó, O.; Yáñez, M. Infrared Spectra of Cyanoacetaldehyde ($NCCH_2CHO$): A Potential Prebiotic Compound of Astrochemical Interest. *ChemPhysChem* **2013**, *14*, 2764−2771.
(9) Møllendal, H.; Margulès, L.; Motiyenko, R. A.; Larsen, N. W.; Guillemin, J.-C. Rotational Spectrum and Conformational Composition of Cyanoacetaldehyde, a Compound of Potential Prebiotic and Astrochemical Interest. *J. Phys. Chem. A* **2012**, *116*, 4047−4056.
(10) Horn, A.; Møllendal, H.; Guillemin, J.-C. A Quantum Chemical Study of the Generation of a Potential Prebiotic Compound, Cyanoacetaldehyde, and Related Sulfur Containing Species. *J. Phys. Chem. A* **2008**, *112*, 11009−11016.
(11) Nandi, S.; Calderini, D.; Bloino, J.; Rampino, S.; Barone, V. A Modern-Fortran Program for Chemical Kinetics on Top of Anharmonic Vibrational Calculations. *Lect. Notes Comput. Sci.* **2019**, *11624*, 401−412.
(12) Nandi, S.; Ballotta, B.; Rampino, S.; Barone, V. A General User-Friendly Tool for Kinetic Calculations of Multi-Step Reactions within the Virtual Multifrequency Spectrometer Project. *Appl. Sci.* **2020**, *10*, 1872.
(13) Lupi, J.; Puzzarini, C.; Cavallotti, C.; Barone, V. State-of-the-Art Quantum Chemistry Meets Variable Reaction Coordinate Transition State Theory to Solve the Puzzling Case of the H_2S + Cl System. *J. Chem. Theory Comput.* **2020**, *16*, 5090−5104.
(14) Barone, V.; Ceselin, G.; Fusè, M.; Tasinato, N. Accuracy Meets Interpretability for Computational Spectroscopy by Means of Hybrid and Double-Hybrid Functionals. *Front. Chem.* **2020**, *8*, 584203.
(15) Xie, F.; Fusè, M.; Hazrah, A. S.; Jäger, W.; Barone, V.; Xu, Y. Discovering the elusive global minimum in a ternary chiral cluster: rotational spectra of propylene oxide trimer. *Angew. Chem., Int. Ed.* **2020**, *59*, 22427−22430.
(16) Grimme, S. Semiempirical hybrid density functional with perturbative second-order correlation. *J. Chem. Phys.* **2006**, *124*, 034108.
(17) Biczysko, M.; Panek, P.; Scalmani, G.; Bloino, J.; Barone, V. Harmonic and Anharmonic Vibrational Frequency Calculations with the Double-Hybrid B2PLYP Method: Analytic Second Derivatives and Benchmark Studies. *J. Chem. Theory Comput.* **2010**, *6*, 2115−2125.
(18) Grimme, S.; Antony, J.; Ehrlich, S.; Krieg, H. A consistent and accurate ab initio parametrization of density functional dispersion correction (DFT-D) for the 94 elements H-Pu. *J. Chem. Phys.* **2010**, *132*, 154104.
(19) Papajak, E.; Zheng, J.; Xu, X.; Leverentz, H. R.; Truhlar, D. G. Perspectives on Basis Sets Beautiful: Seasonal Plantings of Diffuse Basis Functions. *J. Chem. Theory Comput.* **2011**, *7*, 3027−3034.
(20) Fukui, K. The path of chemical reactions - the IRC approach. *Acc. Chem. Res.* **1981**, *14*, 363−368.
(21) Kozuch, S.; Martin, J. M. L. DSD-PBEP86: in search of the best double-hybrid DFT with spin-component scaled MP2 and dispersion corrections. *Phys. Chem. Chem. Phys.* **2011**, *13*, 20104−20107.
(22) Møller, C.; Plesset, M. S. Note on an Approximation Treatment for Many-Electron Systems. *Phys. Rev.* **1934**, *46*, 618−622.
(23) Purvis, G. D.; Bartlett, R. J. A full coupled-cluster singles and doubles model: The inclusion of disconnected triples. *J. Chem. Phys.* **1982**, *76*, 1910−1918.
(24) Puzzarini, C.; Biczysko, M.; Barone, V.; Largo, L.; Peña, I.; Cabezas, C.; Alonso, J. L. Accurate Characterization of the Peptide Linkage in the Gas Phase: A Joint Quantum-Chemical and Rotational Spectroscopy Study of the Glycine Dipeptide Analogue. *J. Phys. Chem. Lett.* **2014**, *5*, 534−540.
(25) Puzzarini, C.; Biczysko, M. Microsolvation of 2-Thiouracil: Molecular Structure and Spectroscopic Parameters of the Thiouracil−Water Complex. *J. Phys. Chem. A* **2015**, *119*, 5386−5395.
(26) Spada, L.; Tasinato, N.; Bosi, G.; Vazart, F.; Barone, V.; Puzzarini, C. On the competition between weak OH·····F and CH·····F hydrogen bonds, in cooperation with CH·····O contacts, in the difluoromethane−tert-butyl alcohol cluster. *J. Mol. Spectrosc.* **2017**, *337*, 90−95.
(27) Alessandrini, S.; Barone, V.; Puzzarini, C. Extension of the "Cheap" Composite Approach to Noncovalent Interactions: The jun-ChS Scheme. *J. Chem. Theory Comput.* **2020**, *16*, 988−1006.
(28) Salta, Z.; Tasinato, N.; Lupi, J.; Boussessi, R.; Balbi, A.; Puzzarini, C.; Barone, V. Exploring the Maze of $C_2N_2H_5$ Radicals and Their Fragments in the Interstellar Medium with the Help of Quantum-Chemical Computations. *ACS Earth Space Chem.* **2020**, *4*, 774−782.
(29) Dunning, T. H. Gaussian basis sets for use in correlated molecular calculations. I. The atoms boron through neon and hydrogen. *J. Chem. Phys.* **1989**, *90*, 1007−1023.
(30) Woon, D. E.; Dunning, T. H. Gaussian basis sets for use in correlated molecular calculations. V. Core-valence basis sets for boron through neon. *J. Chem. Phys.* **1995**, *103*, 4572−4585.
(31) Frisch, M. J.; et al. *Gaussian 09*, Revision A.02; Gaussian Inc: Wallingford CT, 2016.
(32) Stanton, J. F.; Gauss, J.; Cheng, L.; Harding, M. E.; Matthews, D. A.; Szalay, P. G. *CFOUR, Coupled-Cluster Techniques for Computational Chemistry, a Quantum-Chemical Program Package*.
(33) Matthews, D. A.; Cheng, L.; Harding, M. E.; Lipparini, F.; Stopkowicz, S.; Jagau, T.-C.; Szalay, P. G.; Gauss, J.; Stanton, J. F. Coupled-cluster techniques for computational chemistry: The CFOUR program package. *J. Chem. Phys.* **2020**, *152*, 214108.
(34) Rossi, E.; et al. Code interoperability and standard data formats in quantum chemistry and quantum dynamics: The Q5/D5Cost data model. *J. Comput. Chem.* **2014**, *35*, 611−621.
(35) Rampino, S.; Monari, A.; Rossi, E.; Evangelisti, S.; Laganà, A. A priori modeling of chemical reactions on computational grid platforms: Workflows and data models. *Chem. Phys.* **2012**, *398*, 192−198.
(36) Behnke, M.; Medvedev, I.; Winnewisser, M.; De Lucia, F. C.; Herbst, E. The Millimeter-and Submillimeter-Wave Spectrum of Oxiranecarbonitrile. *Astrophys. J. Suppl.* **2004**, *152*, 97−101.
(37) Rampino, S.; Faginas Lago, N.; Laganà, A.; Huarte-Larrañaga, F. An extension of the grid empowered molecular simulator to quantum reactive scattering. *J. Comput. Chem.* **2012**, *33*, 708−714.
(38) Rampino, S.; Skouteris, D.; Laganà, A. Microscopic branching processes: The O + O_2 reaction and its relaxed potential representations. *Int. J. Quantum Chem.* **2010**, *110*, 358−367.
(39) Rampino, S.; Skouteris, D.; Laganà, A. The O + O_2 reaction: quantum detailed probabilities and thermal rate coefficients. *Theor. Chem. Acc.* **2009**, *123*, 249−256.
(40) Laganà, A.; Faginas Lago, N.; Rampino, S.; Huarte-Larrañaga, F.; García, E. Thermal rate coefficients in collinear versus bent transition state reactions: the N + N_2 case study. *Phys. Scr.* **2008**, *78*, 058116.
(41) Rampino, S.; Pastore, M.; Garcia, E.; Pacifici, L.; Laganà, A. On the temperature dependence of the rate coefficient of formation of C from C + CH^+. *Mon. Not. R. Astron. Soc.* **2016**, *460*, 2368−2375.
(42) Pacifici, L.; Pastore, M.; Garcia, E.; Laganà, A.; Rampino, S. A dynamics investigation of the C + CH^+ → C + H reaction on an *ab initio* bond-order like potential. *J. Phys. Chem. A* **2016**, *120*, 5125−5135.
(43) Rampino, S.; Suleimanov, Y. V. Thermal Rate Coefficients for the Astrochemical Process C + CH^+ → $C2^+$ + H by Ring Polymer Molecular Dynamics. *J. Phys. Chem. A* **2016**, *120*, 9887−9893.
(44) Rice, O. K.; Ramsperger, H. C. Theories of Unimolecular Gas Reactions at Low Pressures. *J. Am. Chem. Soc.* **1927**, *49*, 1617−1629.
(45) Kassel, L. S. Studies in Homogeneous Gas Reactions. I. *J. Phys. Chem.* **1928**, *32*, 225−242.
(46) Marcus, R. A. Unimolecular Dissociations and Free Radical Recombination Reactions. *J. Chem. Phys.* **1952**, *20*, 359−364.
(47) Stein, S. E.; Rabinovitch, B. S. Accurate evaluation of internal energy level sums and densities including anharmonic oscillators and hindered rotors. *J. Chem. Phys.* **1973**, *58*, 2438−2445.
(48) Bates, D. R.; Herbst, E. Radiative Association. In *Rate Coefficients in Astrochemistry: Proceedings of a Conference held at Umis, Manchester, U.K. September 21−24, 1987*; Millar, T. J., Williams, D. A., Eds.; Springer Netherlands, 1988, pp 17−40.

https://doi.org/10.1021/acsearthspacechem.1c00013
ACS Earth Space Chem. 2021, 5, 1071−1082

(49) Klippenstein, S. J.; Yang, Y. C.; Ryzhov, V.; Dunbar, R. C. Theory and modeling of ion-molecule radiative association kinetics. *J. Chem. Phys.* **1996**, *104*, 4502−4516.
(50) Herbst, E.; Dunbar, R. C. A global view of radiative association as a function of product size: interstellar implications. *Mon. Not. R. Astron. Soc.* **1991**, *253*, 341−349.
(51) Vuitton, V.; Yelle, R. V.; Lavvas, P.; Klippenstein, S. J. Rapid Association Reactions at Low Pressure: Impact on the Formation of Hydrocarbons on Titan. *Astrophys. J.* **2012**, *744*, 11.
(52) Vazart, F.; Latouche, C.; Skouteris, D.; Balucani, N.; Barone, V. Cyanomethanimine Isomers in Cold Interstellar Clouds: Insights from Electronic Structure and Kinetic Calculations. *Astrophys. J.* **2015**, *810*, 111.
(53) Shingledecker, C. N.; Molpeceres, G.; Rivilla, V. M.; Majumdar, L.; Kästner, J. Isomers in Interstellar Environments. I. The Case of Z- and E-cyanomethanimine. *Astrophys. J.* **2020**, *897*, 158.

https://doi.org/10.1021/acsearthspacechem.1c00013
ACS Earth Space Chem. 2021, 5, 1071−1082